

ON A REACTION-DIFFUSION-ADVECTION GLUCOSE METABOLISM MODEL*

YIWEN TAO[†] AND JUNPING SHI[‡]

Abstract. A reaction-diffusion-advection glucose metabolism model is proposed to describe the spatiotemporal behaviors of glucose in the pancreatic islet. The global existence and boundedness of the solution to the model are proved, and the existence and uniqueness of the positive steady state are established. Spatiotemporal sensitivity index and correlation index are proposed to identify high-impact physiological factors and illustrate parameter interdependency. Additionally, different stages of glucose metabolism such as hyperinsulinemia, hypoglycemia, euglycemia, and diabetes are simulated to demonstrate the system's dynamics under varying physiological conditions. These findings provide valuable guidance in the therapeutic process, aiding in the development of effective interventions.

Key words. glucose metabolism model, reaction-diffusion-advection equation, spatial heterogeneity, steady state, spatiotemporal sensitivity and correlation

MSC codes. 35J56, 92C30, 92C50

DOI. 10.1137/23M1619459

1. Introduction. Diabetes mellitus is a chronic disorder characterized by persistent hyperglycemia, necessitating lifelong care to prevent or delay debilitating complications and premature mortality. According to the International Diabetes Federation (IDF), the prevalence of diabetes in adults has been steadily rising in recent decades. It is projected to surge from 415 million cases in 2015 to over 640 million cases by 2040, making diabetes the seventh-leading cause of death [17, 31, 6]. Recent research indicates that individuals and patients with diabetes are disproportionately susceptible to the impact of COVID-19. Concurrent comorbidities further amplify the risk of hospitalization and mortality [13]. Consequently, significant attention is directed towards the effective management of diabetes, as it is closely associated with various comorbidities, including vision loss, renal failure, retinopathy, and strokes.

The body's glucose-insulin regulation mechanism, known as glucose homeostasis, maintains glucose and insulin levels within narrow ranges when functioning properly. The normal glucose range throughout the day is $70 - 130 \text{ mg/dL}$, with a fasting range of $70 - 100 \text{ mg/dL}$. Fasting insulin levels typically fall within $5 - 25 \text{ } \mu\text{U/mL}$, while nonfasting levels has a range of $30 - 230 \text{ } \mu\text{U/mL}$. Achieving these ranges relies on the precise control system of glucose-insulin regulation, with pancreatic β -cells serving as glucose sensors and adjusting insulin secretion accordingly. The field of artificial/bioartificial pancreas systems recognizes the crucial role of glucose-induced insulin secretion. As a result, various mathematical models [28, 8, 3, 14, 23, 30, 21, 10]

*Received by the editors November 27, 2023; accepted for publication (in revised form) January 3, 2025; published electronically April 10, 2025.

<https://doi.org/10.1137/23M1619459>

Funding: The work of the first author was supported by National Natural Science Foundation of China grant 12201577 and the China Postdoctoral Science Foundation 2024M762971. The work of the second author was supported by US-NSF grants DMS-1853598 and OCE-2207343.

[†]School of Mathematics and Statistics, Zhengzhou University, Zhengzhou, Henan 450001, China (taoyiwen@zzu.edu.cn).

[‡]Department of Mathematics, William & Mary, Williamsburg, VA 23187-8795 USA (jxshix@wm.edu).

have been developed to describe the glucose-insulin regulatory system. These models are widely used, for example, to estimate glucose effectiveness and insulin sensitivity through intravenous glucose tolerance tests (IVGTT). Enhancing our quantitative understanding of glucose-insulin metabolism will contribute to more effective preventive and therapeutic interventions for diabetes.

Recent advancements have expanded our knowledge of the spatiotemporal dynamics of glucose-insulin metabolism, from insulin secretory granules (SG) that dominate insulin secretion [19, 18], to the exocytotic machinery involved in secretion, trafficking, and membrane repair of insulin [32, 7]. Ohara-Imaizumi et al. [18] utilized total internal reflection fluorescence (TIRF) imaging analysis to uncover spatially heterogeneous differences in the processes of first- and second-phase insulin exocytosis in pancreatic β cells. Zhu et al. [32] investigated the changes in spatial distribution of SGs and visualized the spatiotemporal mobilization of SG populations and single SG fusion dynamics following glucose stimulation using TIRF. Each SG exhibits distinct behavior based on its position, size, and time, resulting in heterogeneity among SGs in different states and generating rich dynamics.

Pioneering works on modeling glucose-insulin metabolism have primarily focused on spatially homogeneous dynamical models, with or without time delays. While this approach facilitates the derivation of analytical results, it overlooks the spatial heterogeneity and spatial effect on various indices. Recent studies have detailed the exocytotic mechanisms of insulin SG, which play a crucial role in insulin secretion and demonstrate spatial heterogeneity during different phases. Each SG exhibits distinct behaviors influenced by its position, size, and timing, contributing to the intricate spatiotemporal dynamics observed in glucose-insulin metabolism. Consequently, employing a spatial model to describe the spatiotemporal patterns of glucose and insulin across various times and locations is not only more realistic but also more precise.

The objective of this paper is to develop a reaction-diffusion-advection glucose-insulin model that (1) focuses on quantitative modeling of local dynamics, incorporating detailed spatial distribution of relevant concentrations, (2) calculates spatiotemporal sensitivity and correlation indices to simplify the complexity of glucose metabolism and identify the significant factors influencing glucose homeostasis at an average human level, (3) simulates multiple stages of diabetes, including hyperinsulinemia, hypoglycemia, and diabetes. These findings will aid in the interpretation of experimental data, elucidate the metabolic process, and guide therapeutic schedules.

2. Model. Many factors affect a person's blood sugar level. The body's homeostatic mechanism of blood sugar regulation (known as glucose homeostasis), when operating normally, restores the blood sugar level to a narrow range [4]. The endocrine pancreas plays a key role in the pathogenic process of T2 DM, which is an elongated and tapered organ and is partitioned into the head, body, and tail [22]. It is in the endocrine pancreas that insulin is directly secreted into the bloodstream in response to an elevation in blood glucose, initiating the uptake of glucose by muscle and adipose tissue.

We aim to construct a partial differential equation model to describe the spatiotemporal evolution of the spatial concentrations of glucose and insulin in pancreas. Glucose and peripheral insulin enter the pancreas with the blood flow and are distributed through capillaries. The elongated shape of the pancreas allows us to assume that it occupies a one-dimensional spatial domain with length $L > 0$ in which the arterial blood flows into the head ($x = 0$) and flows out of the tail ($x = L$) of the hepatic portal vein. Dynamic imaging of pancreatic islet blood flow in [16] shows

that there mainly exist two predominant flow patterns: inner-to-outer (diffusion) and top-to-bottom (convection). Since the blood flux maintains a constant rate in an individual vein, it is natural to assume that the rates of diffusion and advection of glucose and insulin, which take the blood flow as a carrier, also keep uniform from the starting point ($x = 0$) to the end ($x = L$).

Glucose dynamics. Let $G(x, t)$ denote the concentration of plasma glucose at location x and time t . The blood flow carries the glucose with velocity v_G in the positive x direction and with diffusivity d_G in the vein. The net hepatic glucose production is the difference between the rates of glucose production and uptake under zero glucose conditions, which is assumed to be at a constant rate G_{in} . Glucose uptake is accomplished via two mechanisms: insulin-mediated glucose uptake, which occurs in insulin-sensitive tissues (i.e., liver, muscle, and adipocytes), and noninsulin-mediated glucose uptake, which occurs in both insulin-sensitive and noninsulin-sensitive tissues (i.e., brain, blood cells, nerve, etc). The insulin-independent uptake is proportional to glucose concentration G with a parameter of glucose effectiveness μ_G ; and the insulin-dependent glucose uptake is proportional to both glucose concentration G and blood insulin concentration I with an insulin sensitivity c . Bergman et al. [15] provided experimental evidence for this relationship using the glucose clamp technique. Therefore, the rate of change of plasma glucose satisfies the following metabolic relationship:

rate change of glucose = glucose diffusion + glucose advection + production – uptake.

For the boundary conditions, we assume that no blood glucose flow in or out at $x = 0$ and all glucose flow out of the vein at $x = L$. Taking together these assumptions results in the following reaction-diffusion-advection equation of G with Danckwerts boundary condition:

$$(2.1) \quad \begin{cases} G_t = d_G G_{xx} - v_G G_x + G_{in} - cIG - \mu_G G, & 0 < x < L, t > 0, \\ d_G G_x(0, t) - v_G G(0, t) = 0, & t > 0, \\ G_x(L, t) = 0, & t > 0. \end{cases}$$

Insulin dynamics. Insulin kinetics are the intermediate step between the secretion of insulin and its action on glucose fluxes, as for a given insulin secretion response following a glucose stimulus insulin concentration is determined by insulin distribution and clearance. Our main concern is the spatio-temporal evolution of fasting insulin levels in peripheral blood. Let $I(x, t)$ describe the concentration of insulin in the blood vein at location x and time t . Due to the inner-to-outer movement and top-to-bottom transport of the blood, there is diffusion (with diffusivity d_I) and advection (with velocity v_I) of insulin in the vein. When the glucose level is high, insulin is secreted into the blood; and when the glucose level is low, the secretion of insulin is inhibited. The intrinsic growth of insulin depends on the concentration of plasma glucose G in the hepatic portal vein, and it takes a Michaelis–Menten type functional response form $\frac{aG^n}{(m+G)^n}$ with $n = 1$ or 2 , where a is the maximum production rate of plasma insulin, and m is the half-saturation constant. The insulin clearance rate is denoted by μ_I , representing the combined insulin uptake at the liver, kidneys, and insulin receptors. The following relationship describes the process of insulin metabolism:

$$\begin{aligned} &\text{rate of change of insulin} \\ &= \text{glucose diffusion} + \text{insulin advection} + \text{production} - \text{clearance}. \end{aligned}$$

Combining these assumptions and similar boundary conditions as the ones for glucose, the dynamics of I is described by

TABLE 1
Model variables and parameters with physiological meanings and values.

Symbol	Meaning	Value	Unit	Ref
G	glucose concentration	varies	$mg \cdot dl^{-1}$	
I	insulin concentration	varies	$\mu U \cdot ml^{-1}$	
L	length of vein	15	cm	[9]
μ_G	noninsulin-mediated glucose uptake rate	0.001	min^{-1}	[27]
μ_I	insulin clearance rate	0.3	min^{-1}	[27]
v_G	glucose-cell advection coefficient	0.5	$cm \cdot min^{-1}$	[16]
v_I	insulin-cell advection coefficient	0.5	$cm \cdot min^{-1}$	[16]
d_G	glucose-cell diffusion coefficient	0.0013	$cm^2 \cdot min^{-1}$	[26, 1]
d_I	insulin-cell diffusion coefficient	0.00018	$cm^2 \cdot min^{-1}$	[11]
m	half-saturation constant	20000	$mg \cdot dl^{-1}$	[27]
G_{in}	net hepatic glucose production rate	0.6	$mg \cdot dl^{-1} \cdot min^{-1}$	[27]
a	maximum insulin production rate	6.27	$\mu U \cdot ml^{-1} \cdot min^{-1}$	[23]
c	insulin sensitivity	0.0005	$\mu U^{-1} \cdot ml \cdot min^{-1}$	[27]
n	Michaelis–Menten exponent	1	-	

$$(2.2) \quad \begin{cases} I_t = d_I I_{xx} - v_I I + \frac{aG^n}{(m+G)^n} - \mu_I I, & 0 < x < L, t > 0, \\ d_I I_x(0, t) - v_I I(0, t) = 0, & t > 0, \\ I_x(L, t) = 0, & t > 0. \end{cases}$$

All the system variables and parameters of the model and their physiological significance are listed in Table 1. The full model of glucose and insulin in the hepatic portal vein takes the following form:

$$(2.3) \quad \begin{cases} G_t = d_G G_{xx} - v_G G_x + G_{in} - cIG - \mu_G G, & 0 < x < L, t > 0, \\ I_t = d_I I_{xx} - v_I I_x + \frac{aG^n}{(m+G)^n} - \mu_I I, & 0 < x < L, t > 0, \\ d_G G_x(0, t) - v_G G(0, t) = 0, & t > 0, \\ d_I I_x(0, t) - v_I I(0, t) = 0, & t > 0, \\ G_x(L, t) = I_x(L, t) = 0, & t > 0, \\ G(x, 0) = G_0(x), I(x, 0) = I_0(x), & 0 < x < L, t = 0. \end{cases}$$

3. Dynamics. In this section, we consider the dynamical behavior of solutions of (2.3). First, we prove the global existence of solution of (2.3) and establish some a priori bounds of the solutions. The boundedness of solution directly implies the existence of a positive steady state solution. Second, we show the uniqueness of the positive steady state solution, and we also show that the positive steady state solution is globally asymptotically stable under some additional conditions.

For $d > 0$, $v \geq 0$, and $B > 0$, we define the roots of quadratic equation $d\lambda^2 - v\lambda - B = 0$ to be

$$(3.1) \quad \lambda_+(d, v, B) = \frac{v + \sqrt{v^2 + 4dB}}{2d}, \quad \lambda_-(d, v, B) = \frac{v - \sqrt{v^2 + 4dB}}{2d},$$

and for $0 \leq x \leq L$,

$$(3.2) \quad w(x; d, v, B) = \frac{v(\lambda_+ e^{\lambda_-(x-L)} - \lambda_- e^{\lambda_+(x-L)})}{\lambda_+ e^{-\lambda_- L}(d\lambda_- - v) - \lambda_- e^{-\lambda_+ L}(d\lambda_+ - v)},$$

where $\lambda_{\pm} = \lambda_{\pm}(d, v, B)$ are defined as in (3.1).

LEMMA 3.1. *If $d, A, B > 0$, $v \geq 0$, and $u(x, t)$ satisfies*

$$(3.3) \quad \begin{cases} u_t \leq (\geq) du_{xx} - vu_x - Bu + A, & 0 < x < L, t > 0, \\ du_x(0, t) - vu(0, t) = u_x(L, t) = 0, & t > 0, \\ u(x, 0) = u_0(x), \end{cases}$$

then for any $\epsilon > 0$, there exists $T_u > 0$ such that $u(x, t) \leq u^*(x) + \epsilon$ ($\geq u^*(x) - \epsilon$) for $(x, t) \in [0, L] \times [T_u, \infty)$, where

$$u^*(x) = \frac{A}{B}(w(x; d, v, B) + 1),$$

and $w(x; d, v, B)$ is defined in (3.2). Moreover, $u^*(x)$ is strictly increasing for $x \in [0, L]$, and $0 < u^*(0) \leq u^*(x) \leq u^*(L) < A/B$.

Proof. We only prove the \leq case as the other one is similar. From the comparison principle of parabolic equations, it is easy to verify that $u(x, t) \leq u^*(x, t)$ where $u^*(x, t)$ is the solution of

$$(3.4) \quad \begin{cases} u_t = du_{xx} - vu_x - Bu + A, & 0 < x < L, t > 0, \\ du_x(0, t) - vu(0, t) = u_x(L, t) = 0, & t > 0, \\ u(x, 0) = u_0(x). \end{cases}$$

Then we have $\limsup_{t \rightarrow \infty} u(x, t) \leq \limsup_{t \rightarrow \infty} u^*(x, t) = u^*(x)$, where $u^*(x)$ is the unique steady state solution of (3.4) satisfying

$$(3.5) \quad du_{xx} - vu_x - Bu + A = 0, \quad 0 < x < L, \quad du_x(0) - vu(0) = u_x(L) = 0.$$

It is easy to verify that $\bar{u}(x) = A/B$ and $\underline{u}(x) = 0$ are a pair of upper and lower solutions of (3.5), hence there exists a solution $\tilde{u}(x)$ satisfying $\underline{u}(x) \leq \tilde{u}(x) \leq \bar{u}(x)$. Since the solution of (3.5) is unique as it is linear, we have $\tilde{u}(x) = u^*(x)$ and $\underline{u}(x) \leq u^*(x) \leq \bar{u}(x)$. From the maximum principle for elliptic equations, we can verify that $u^*(x)$ is strictly increasing for $x \in [0, L]$, and $u^*(0) \leq u^*(x) \leq u^*(L)$. From the strong maximum principle, we have $0 < u^*(0) \leq u^*(x) \leq u^*(L) < A/B$. \square

The following results show that the solutions of (2.3) always exist for all $t > 0$ and are ultimately uniformly bounded.

THEOREM 3.2. *Suppose that $G_{in}, d_{G,I}, \mu_{G,I}, a, c, e, L > 0$, and $v_{G,I} \geq 0$.*

1. *If $G_0(x) \geq 0$, $I_0(x) \geq 0$ for $x \in [0, L]$, then (2.3) has a unique solution $(G(x, t), I(x, t))$ such that $G(x, t) > 0$, $I(x, t) > 0$ for $t \in (0, \infty)$, and $x \in [0, L]$.*
2. *Any solution $(G(x, t), I(x, t))$ of (2.3) satisfies*

$$\begin{aligned} G_*(x) &\leq \liminf_{t \rightarrow \infty} G(x, t) \leq \limsup_{t \rightarrow \infty} G(x, t) \leq G^*(x), \quad x \in [0, L], \\ I_*(x) &\leq \liminf_{t \rightarrow \infty} I(x, t) \leq \limsup_{t \rightarrow \infty} I(x, t) \leq I^*(x), \quad x \in [0, L], \end{aligned}$$

where

$$\begin{aligned} G^*(x) &= \frac{G_{in}}{\mu_G}(w(x; d_G, v_G, \mu_G) + 1), \quad I^*(x) = \frac{a}{\mu_I}(w(x; d_I, v_I, \mu_I) + 1), \\ G_*(x) &= \frac{G_{in}}{\mu_G^*}(w(x; d_G, v_G, \mu_G) + 1), \quad I_*(x) = \frac{a}{\mu_I^*}(w(x; d_I, v_I, \mu_I) + 1), \end{aligned}$$

with

$$\begin{aligned}\mu_G^* &= \frac{\mu_G \mu_I + ac(w(L; d_I, v_I, \mu_I) + 1)}{\mu_I}, \\ \mu_I^* &= \frac{\mu_I G_{in}^n (w(0; d_G, v_G, \mu_G) + 1)^n}{[G_{in}(w(0; d_G, v_G, \mu_G) + 1) + \mu_G m]^n}.\end{aligned}$$

Moreover, (2.3) has at least one positive steady state solution $(G_S(x), I_S(x))$ satisfying

$$(3.6) \quad G_*(x) \leq G_S(x) \leq G^*(x), \quad I_*(x) \leq I_S(x) \leq I^*(x), \quad x \in [0, L].$$

3. For any solution $(G(x, t), I(x, t))$ of (2.3),

$$(3.7) \quad \limsup_{t \rightarrow \infty} \int_0^L [G(x, t) + I(x, t)] dx \leq \frac{(G_{in} + a)L}{\min\{\mu_G, \mu_I\}}.$$

Proof. 1. Define

$$f_1(G, I) = G_{in} - cIG - \mu_G G, \quad f_2(G, I) = \frac{aG^n}{(m + G)^n} - \mu_I I,$$

then $\frac{\partial f_1}{\partial I} = -cG < 0$, and $\frac{\partial f_2}{\partial G} = \frac{naeG^{n-1}}{(m+G)^{n+1}} > 0$ in $\mathbb{R}_+^2 = \{G > 0, I > 0\}$, which implies that (2.3) is a mixed quasimonotone system. According to Pao [20, Definition 8.1.2], a pair of functions (\bar{G}, \bar{I}) and $(\underline{G}, \underline{I})$ in $C(\bar{D}_T) \cap C^{1,2}(D_T)$ are called ordered upper and lower solutions of (2.3) if they satisfy the inequalities

$$(3.8) \quad \begin{cases} \bar{G}_t - d_G \bar{G}_{xx} + v_G \bar{G}_x - f_1(\bar{G}, \bar{I}) \geq 0 \geq \underline{G}_t - d_G \underline{G}_{xx} + v_G \underline{G}_x - f_1(\underline{G}, \bar{I}), \\ \bar{I}_t - d_I \bar{I}_{xx} + v_I \bar{I}_x - f_2(\bar{G}, \bar{I}) \geq 0 \geq \underline{I}_t - d_I \underline{I}_{xx} + v_I \underline{I}_x - f_2(\underline{G}, \underline{I}), \\ -d_G \bar{G}_x(0, t) + v_G \bar{G}(0, t) \geq 0 \geq -d_G \underline{G}_x(0, t) + v_G \underline{G}(0, t), \\ -d_I \bar{I}_x(0, t) + v_I \bar{I}(0, t) \geq 0 \geq -d_I \underline{I}_x(0, t) + v_I \underline{I}(0, t), \\ \bar{G}_x(L, t) \geq 0 \geq \underline{G}_x(L, t), \quad \bar{I}_x(L, t) \geq 0 \geq \underline{I}_x(L, t), \\ \bar{G}(x, t) \geq \underline{G}(x, t), \quad \bar{I}(x, t) \geq \underline{I}(x, t), \end{cases}$$

with the initial conditions $\bar{G}(x, 0) \geq G_0(x) \geq \underline{G}(x, 0)$, $\bar{I}(x, 0) \geq I_0(x) \geq \underline{I}(x, 0)$. Let $G_M = \max_{0 \leq x \leq L} G_0(x)$ and $I_M = \max_{0 \leq x \leq L} I_0(x)$. Define

$$(\bar{G}, \bar{I}) = \left(\frac{\max\{G_{in}, G_M\} e^{\frac{v_G}{d_G} x}}{\mu_G}, \frac{\max\{a, I_M\} e^{\frac{v_I}{d_I} x}}{\mu_I} \right).$$

Then the functions (\bar{G}, \bar{I}) and $(\underline{G}, \underline{I}) = (0, 0)$ are a pair of ordered upper and lower solutions to (2.3), as they satisfy

$$(3.9) \quad \begin{cases} \bar{G}_t - d_G \bar{G}_{xx}(x, t) + v_G \bar{G}_x(x, t) - f_1(\bar{G}(x, t), \underline{I}(x, t)) \geq G_{in} e^{\frac{v_G}{d_G} x} - G_{in} \geq 0 \\ \quad > -G_{in} = \underline{G}_t - d_G \underline{G}_{xx}(x, t) + v_G \underline{G}_x(x, t) - f_1(\underline{G}(x, t), \bar{I}(x, t)), \\ \bar{I}_t - d_I \bar{I}_{xx}(x, t) + v_I \bar{I}_x(x, t) - f_2(\bar{G}(x, t), \bar{I}(x, t)) \geq a \left(e^{\frac{v_I}{d_I} x} - \frac{\bar{G}^n}{(m + \bar{G})^n} \right) \\ \quad > 0 = \underline{I}_t - d_I \underline{I}_{xx}(x, t) + v_I \underline{I}_x(x, t) - f_2(\underline{G}(x, t), \underline{I}(x, t)), \end{cases}$$

and the boundary conditions and initial values

$$(3.10) \quad \begin{cases} d_G \bar{G}_x(0, t) - v_G \bar{G}(0, t) = 0 = d_G \underline{G}_x(0, t) - v_G \underline{G}(0, t), \\ d_I \bar{I}_x(0, t) - v_I \bar{I}(0, t) = 0 = d_I \underline{I}_x(0, t) - v_I \underline{I}(0, t), \\ \frac{\max\{G_{in}, G_M\} v_G}{\mu_G d_G} = \bar{G}_x(L, t) \geq 0 = \underline{G}_x(L, t), \\ \frac{\max\{a, I_M\} v_I e^{\frac{v_I}{a_I} L}}{\mu_I d_I} = \bar{I}_x(L, t) \geq 0 = \underline{I}_x(L, t), \\ \bar{G}(x, 0) \geq G_0(x) \geq \underline{G}(x, 0), \bar{I}(x, 0) \geq I_0(x) \geq \underline{I}(x, 0). \end{cases}$$

According to Theorem 8.3.3 in [20], model (2.3) has a unique globally defined solution $(G(x, t), I(x, t))$ which satisfies

$$0 \leq G(x, t) \leq \bar{G}(x), \quad 0 \leq I(x, t) \leq \bar{I}(x), \quad 0 \leq x \leq L, t \geq 0.$$

The strong maximum principle implies that $G(x, t), I(x, t) > 0$ when $t > 0$ for all $x \in [0, L]$.

2. To consider the global boundedness, we observe that $G(x, t)$ satisfies

$$(3.11) \quad G_t \leq d_G G_{xx} - v_G G_x + G_{in} - \mu_G G, \quad 0 \leq x \leq L, t > 0.$$

From Lemma 3.1, we have $G(x, t) \leq G^*(x, t)$, where $G^*(x, t)$ is the solution of

$$(3.12) \quad \begin{cases} G_t = d_G G_{xx} - v_G G_x + G_{in} - \mu_G G, & 0 \leq x \leq L, t > 0, \\ d_G G_x(0, t) - v_G G(0, t) = G_x(L, t) = 0, & t > 0, \\ G(x, 0) = G_0(x), \end{cases}$$

then $\limsup_{t \rightarrow \infty} G(x, t) \leq \limsup_{t \rightarrow \infty} G^*(x, t) = G^*(x)$. For any $\varepsilon > 0$, there exists $T_1 > 0$, such that $G(x, t) \leq G^*(x) + \varepsilon$ for $x \in [0, L] \times [T_1, \infty)$. Similarly, $I(x, t)$ satisfies

$$(3.13) \quad I_t \leq d_I I_{xx} - v_I I_x + a - \mu_I I, \quad 0 \leq x \leq L, t > 0.$$

Hence from Lemma 3.1, $\limsup_{t \rightarrow \infty} I(x, t) \leq \limsup_{t \rightarrow \infty} I^*(x, t) = I^*(x)$, where $I^*(x, t)$ is the solution of

$$(3.14) \quad \begin{cases} I_t = d_I I_{xx} - v_I I_x - \mu_I I + a, & 0 \leq x \leq L, t > 0, \\ d_I I_x(0, t) - v_I I(0, t) = I_x(L, t) = 0, & t > 0, \\ I(x, 0) = I_0(x). \end{cases}$$

Then for $\varepsilon > 0$, there exists $T_2 > 0$, such that $I(x, t) \leq I^*(x) + \varepsilon$ for $x \in [0, L] \times [T_2, \infty)$.

Moreover, $G(x, t)$ satisfies

$$(3.15) \quad G_t \geq d_G G_{xx} - v_G G_x - (c\bar{I}_{max} + c\varepsilon + \mu_G)G + G_{in}, \quad 0 \leq x \leq L, t > T_2,$$

with $\bar{I}_{max} = \frac{a}{\mu_I}(w(L; d_I, v_I, \mu_I) + 1)$. From Lemma 3.1, $\liminf_{t \rightarrow \infty} G(x, t) \geq \liminf_{t \rightarrow \infty} G_*(x, t) = G_*(x)$. Here $G_*(x, t)$ is the solution of

$$(3.16) \quad \begin{cases} G_t = d_G G_{xx} - v_G G_x - (c\bar{I}_{max} + \mu_G)G + G_{in}, & 0 \leq x \leq L, t > 0, \\ d_G G_x(0, t) - v_G G(0, t) = G_x(L, t) = 0, & t > 0, \\ G(x, 0) = G_0(x). \end{cases}$$

Similarly, $I(x, t)$ satisfies

$$(3.17) \quad I_t \geq d_I I_{xx} - v_I I_x - \mu_I I + \frac{a(G^*(0) + \epsilon)^n}{(G^*(0) + \epsilon + m)^n}, \quad 0 \leq x \leq L, \quad t > T_1.$$

We have $\liminf_{t \rightarrow \infty} I(x, t) \geq \liminf_{t \rightarrow \infty} I_*(x, t) = I_*(x)$. Here, $I_*(x, t)$ is the solution of

$$(3.18) \quad \begin{cases} I_t = d_I I_{xx} - v_I I_x - \mu_I I + \frac{aG^*(0)^n}{(G^*(0) + m)^n}, & 0 \leq x \leq L, \quad t > 0, \\ d_I I_x(0, t) - v_I I(0, t) = I_x(L, t) = 0, & t > 0, \\ I(x, 0) = I_0(x). \end{cases}$$

It is also easy to verify that $(G^*(x), I^*(x))$ and $(G_*(x), I_*(x))$ are a pair of ordered upper and lower solutions of the steady state equation corresponding to (2.3). Hence, from Theorem 8.10.2 of [20], there exists at least one positive steady state solution of (2.3) satisfying (3.6).

3. By using (2.3), we obtain that

$$(3.19) \quad \begin{aligned} \frac{d}{dt} \int_0^L (G + I) \, dx &\leq (G_{in} + a)L - \int_0^L (cGI + \mu_G G + \mu_I I) \, dx, \\ &\leq (G_{in} + a)L - \min\{\mu_G, \mu_I\} \int_0^L (G + I) \, dx, \end{aligned}$$

which implies (3.7). \square

In Theorem 3.2, we have shown that system (2.3) always has a positive steady state solution, which satisfies the following elliptic system:

$$(3.20) \quad \begin{cases} d_G G_{xx} - v_G G_x + G_{in} - cIG - \mu_G G = 0, & 0 < x < L, \\ d_I I_{xx} - v_I I_x + \frac{aG^n}{(m + G)^n} - \mu_I I = 0, & 0 < x < L, \\ d_G G_x(0) - v_G G(0) = G_x(L) = 0, \\ d_I I_x(0) - v_I I(0) = I_x(L) = 0. \end{cases}$$

To prove the uniqueness of positive solution to (3.20), we recall some results on the following eigenvalue problem:

$$(3.21) \quad \begin{cases} -d\phi''(x) + v\phi'(x) + p(x)\phi = \lambda\phi, & 0 < x < L, \\ d\phi'(0) - v\phi(0) = \phi'(L) = 0. \end{cases}$$

Here $d > 0$, $v \geq 0$, and $p(x) \in L^\infty(0, L)$. We also define a function space

$$(3.22) \quad X(d, v) = \{\varphi \in C^2[0, L] : d\varphi_x(0) - v\varphi(0) = \varphi_x(L) = 0\},$$

and a linear operator $L(d, v, p) : X(d, v) \rightarrow C[0, L]$ by

$$(3.23) \quad L(d, v, p)\phi = -d\phi''(x) + v\phi'(x) + p(x)\phi.$$

Then we have the following properties for the eigenvalues [29].

LEMMA 3.3. Suppose that $d > 0$, $v \geq 0$ and $p(x) \in L^\infty(0, L)$.

1. The eigenvalue problem (3.21) has a sequence of eigenvalues

$$\lambda_1 < \lambda_2 \leq \lambda_3 \leq \dots \leq \lambda_n \leq \dots$$

and $\lim_{n \rightarrow \infty} \lambda_n = \infty$, where the principal eigenvalue λ_1 has the variational characterization

$$\lambda_1(d, v, p) = \inf_{\phi \in H^1(0, L)} \frac{\int_0^L e^{\alpha x} [d(\phi'(x))^2 + p(x)\phi^2(x)] dx + ve^{\alpha L} \phi^2(L)}{\int_0^L e^{\alpha x} \phi^2 dx},$$

with $\alpha = v/d$.

2. When $p(x) \geq (\neq) 0$, we have $\lambda_1(d, v, p) > 0$. Moreover, $L(d, v, p)$ is invertible and $L^{-1}(d, v, p) : C[0, L] \rightarrow X(d, v)$ is strongly positive. That is, for any $\xi \in C[0, L]$, there exists a unique $\eta \in X(d, v)$ such that $L(d, v, p)\eta = \xi$, and when $\xi \geq (\neq) 0$ we have $\eta(x) > 0$ for $x \in [0, L]$.

The following result is a key to our uniqueness result of the positive steady state solution (see [12]).

LEMMA 3.4. Suppose that $d_G, d_I > 0$, $v_G, v_I \geq 0$, $p_G, p_I \in L^\infty(0, L)$, and $f_1, f_2 \in C[0, L]$ satisfying $f_i(x) > 0$ for $x \in [0, L]$ and $i = 1, 2$. Let $L(d_G, v_G, p_G)$ and $L(d_I, v_I, p_I)$ be defined as in (3.23), and let $X(d_G, v_G)$ and $X(d_I, v_I)$ be defined as in (3.22). Then the system of linear equations

$$(3.24) \quad L(d_G, v_G, p_G)\phi = -f_1(x)\psi, \quad L(d_I, v_I, p_I)\psi = f_2(x)\phi,$$

has only the trivial solution $(\phi(x), \psi(x)) \equiv (0, 0)$.

Now we state the uniqueness result of positive steady state solution of (2.3).

THEOREM 3.5. Suppose that $G_{in}, d_{G,I}, \mu_{G,I}, a, c, e, L > 0$ and $v_{G,I} \geq 0$.

1. The system (2.3) has a unique positive steady state solution $(G_S(x), I_S(x))$.
2. Fixing all parameters except a , we have

$$\lim_{a \rightarrow 0^+} G_S(x) = G^*(x), \quad \lim_{a \rightarrow 0^+} I_S(x) = 0.$$

3. Fixing all parameters except G_{in} , we have

$$\begin{aligned} \lim_{G_{in} \rightarrow 0^+} G_S(x) &= 0, & \lim_{G_{in} \rightarrow 0^+} I_S(x) &= 0, \\ \lim_{G_{in} \rightarrow \infty} \frac{G_S(x)}{G_{in}} &= G_\infty(x), & \lim_{G_{in} \rightarrow \infty} I_S(x) &= I^*(x), \end{aligned}$$

where $G_\infty(x)$ is the unique solution of

$$(3.25) \quad \begin{cases} d_G G_{xx} - v_G G_x + 1 - cI^*(x)G - \mu_G G = 0, & 0 < x < L, \\ d_G G_x(0) - v_G G(0) = G_x(L) = 0. \end{cases}$$

Proof. We fix all parameters except $a \geq 0$. We define a nonlinear operator $F : \mathbb{R}^+ \times X(d_G, v_G) \times X(d_I, v_I) \rightarrow C[0, L] \times C[0, L]$:

$$(3.26) \quad F(a, G, I) = \begin{pmatrix} d_G G_{xx} - v_G G_x + G_{in} - cIG - \mu_G G \\ d_I I_{xx} - v_I I_x + \frac{aG^n}{(m+G)^n} - \mu_I I \end{pmatrix}.$$

Then F is a smooth function, and $F(a, G, I) = (0, 0)$ if and only if (G, I) is a solution of (3.20). When $a = 0$, it is obvious that the only nonnegative solution of (3.20) is $(G_S, I_S) = (G^*, 0)$. The Frechét derivative of F at a nonnegative (G_S, I_S) is

$$(3.27) \quad F_{(G,I)}(a, G_S, I_S)(\phi, \psi) = \begin{pmatrix} d_G \phi_{xx} - v_G \phi_x - c I_S \phi - c G_S \psi - \mu_G \phi \\ d_I \psi_{xx} - v_I \psi_x + a f'(G_S) \phi - \mu_I \psi \end{pmatrix},$$

where $f(G) = \frac{G^n}{(m+G)^n}$ and $f'(G) = \frac{mnG^{n-1}}{(m+G)^{n+1}} > 0$ for $G > 0$. Notice that $F_{(G,I)}(a, G_S, I_S)(\phi, \psi) = (0, 0)$ for some $(\phi, \psi) \in X(d_G, v_G) \times X(d_I, v_I)$ is equivalent to

$$(3.28) \quad L(d_G, v_G, p_G)\phi = -cG_S\psi, \quad L(d_I, v_I, p_I)\psi = a f'(G_S)\phi,$$

where $p_G(x) = cG_S(x) + \mu_G > 0$ and $p_I(x) = \mu_I > 0$. From Lemma 3.4, for any nonnegative solution (G_S, I_S) of (3.20) with $G_S(x) > 0$, the only solution of (3.28) is $(\phi, \psi) = (0, 0)$, which implies that $F_{(G,I)}(a, G_S, I_S)$ is invertible. In particular, when $a = 0$, $F_{(G,I)}(0, G^*, 0)$ is invertible. Thus from the implicit function theorem, for a near $a = 0$, there is a unique solution $(G_a(x), I_a(x))$ of $F(a, G, I) = 0$ near $(G^*(x), 0)$. On the other hand, from Theorem 3.2 part 2, for a near $a = 0$, there is a positive solution $(\tilde{G}_a(x), \tilde{I}_a(x))$ of $F(a, G, I) = 0$ satisfying (3.6). Since (3.6) implies that $(\tilde{G}_a(x), \tilde{I}_a(x)) \rightarrow (G^*(x), 0)$ as $a \rightarrow 0^+$, we must have $(\tilde{G}_a(x), \tilde{I}_a(x)) = (G_a(x), I_a(x))$ from the implicit function theorem. Hence for some $a_0 > 0$, there is a positive solution $(G_a(x), I_a(x))$ of $F(a, G, I) = 0$ near $(G^*(x), 0)$ satisfying $(G_a(x), I_a(x)) \rightarrow (G^*(x), 0)$ as $a \rightarrow 0^+$, and all these solutions are on a smooth curve $\Gamma(a_0) = \{(a, G_a(x), I_a(x)) : 0 < a < a_0\}$.

Since $F_{(G,I)}(a, G_S, I_S)$ is invertible for any nonnegative solution (G_S, I_S) of (3.20) with $G_S(x) > 0$ from Lemma 3.4, we can further extend $\Gamma(a_0)$ beyond $a = a_0$. Indeed, because of the bound in (3.6), $\lim_{a \rightarrow a_0^-} (G_a(x), I_a(x))$ exists, and it is a nonnegative solution of $F(a, G, I) = 0$. From the maximum principle of elliptic equations, a nonnegative solution of $F(a, G, I) = 0$ with $a > 0$ and $G_{in} > 0$ must be positive. Hence the implicit function theorem can be applied at $a = a_0$ to extend $\Gamma(a_0)$. Repeatedly applying the argument, we obtain a global curve $\Gamma = \{(a, G_a(x), I_a(x)) : 0 < a < \infty\}$ of positive solutions of $F(a, G, I) = 0$ as the bound (3.6) holds for all $a > 0$.

If for some $a > 0$, there is another positive solution $(\hat{G}_a(x), \hat{I}_a(x))$ of $F(a, G, I) = 0$, then $(\hat{G}_a(x), \hat{I}_a(x))$ also satisfies (3.6) from Theorem 3.2 part 2. Hence we can use the same argument as above to show that $(\hat{G}_a(x), \hat{I}_a(x))$ belongs to another global curve $\hat{\Gamma} = \{(a, \hat{G}_a(x), \hat{I}_a(x)) : 0 < a < \infty\}$. But as $a \rightarrow 0^+$, $(\hat{G}_a(x), \hat{I}_a(x))$ must converge to $(G^*(x), 0)$, which is the unique solution of $F(0, G, I) = 0$. This contradicts with the uniqueness of solution of $F(a, G, I) = 0$ near $(a, G, I) = (0, G^*, 0)$. Therefore, for any $a > 0$, $(G_a(x), I_a(x))$ is the unique positive solution of $F(a, G, I) = 0$. This proves parts 1 and 2.

For part 3, $G_S \rightarrow 0$ as $G_{in} \rightarrow 0^+$ is easy to see as $G^*, G_* \rightarrow 0$ as $G_{in} \rightarrow 0^+$ and (3.6), and that, in turn, also implies $I_S \rightarrow 0$ by using the equation of I_S . On the other hand, when $G_{in} \rightarrow \infty$, $\mu_I^* \rightarrow \mu_I$ and $I_* \rightarrow I^*$ hence $I_S \rightarrow I^*$. The limit of G_S/G_{in} can be obtained using the equation of G_S rescaled by G_{in} . \square

Next, we discuss the global stability of the steady state $(G_S(x), I_S(x))$ when $v_G = v_I = 0$. In that case, (G_S, I_S) is a constant solution where G_S is the unique positive root of $G_{in} - \frac{caG^{n+1}}{\mu_I(m+G)^n} - \mu_G G = 0$ and $I_S = \frac{cG_S^n}{\mu_I(m+G_S)^n}$. With the transformation $\tilde{G} = G - G_S$, $\tilde{I} = I - I_S$, system (2.3) becomes

$$\begin{cases} \tilde{G}_t = d_G(\tilde{G}_{xx} + G_{Sxx}) + G_{in} - cI(G_S + \tilde{G}) - \mu_G(G_S + \tilde{G}), & 0 < x < L, t > 0, \\ \tilde{I}_t = d_I(\tilde{I}_{xx} + I_{Sxx}) + \frac{a(G_S + \tilde{G})^n}{(m + G_S + \tilde{G})^n} - \mu_I(I_S + \tilde{I}), & 0 < x < L, t > 0. \end{cases}$$

To obtain our conclusions, we define the following Lyapunov functional V by

$$V(t) = \int_0^L (\tilde{G}(x, t) + \tilde{I}(x, t)) dx.$$

Let $I(x, t)$ be an arbitrary solution of (2.3) with nonnegative initial values. Then

$$\begin{aligned} \frac{dV(t)}{dt} &= \int_0^L (G_{in} - cI(G_S + \tilde{G}) - \mu_G(G_S + \tilde{G})) dx - d_G \int_0^L \left(\frac{\partial G^2}{\partial x^2} + \frac{\partial G_S^2}{\partial x^2} \right) dx \\ &\quad + \int_0^L \left(\frac{a(G_S + \tilde{G})^n}{(m + G_S + \tilde{G})^n} - \mu_I(I_S + \tilde{I}) \right) dx - d_I \int_0^L \left(\frac{\partial I^2}{\partial x^2} + \frac{\partial I_S^2}{\partial x^2} \right) dx, \\ &\leq \int_0^L \mu_I \left(\frac{a}{\mu_I} - I_S \right) - \int_0^L (cI(G_S + \tilde{G}) + \mu_G \tilde{G}) dx \leq 0. \end{aligned}$$

Note that $\frac{dV(t)}{dt} = 0$ holds if and only if $(\tilde{G}, \tilde{I}) = (0, 0)$. Thus, we conclude that (\tilde{G}, \tilde{I}) converges to $(0, 0)$ uniformly for $x \in [0, L]$ as $t \rightarrow \infty$. We state this global stability results as follows.

THEOREM 3.6. *Suppose that the conditions in Theorem 3.5 are satisfied, and, in addition, $v_G = v_I = 0$. Then the unique positive steady state solution (G_S, I_S) is globally asymptotically stable with respect to (2.3).*

The global asymptotic stability of (G_S, I_S) when the advection rates are not zero is not known, but numerical simulations suggest the stability also holds in that case.

4. Simulations.

4.1. Impact of the insulin secretion and sensitivity on glucose metabolism. Diabetes occurs as a result of insufficient insulin production by the pancreas or the body’s inability to effectively utilize the insulin it produces [5]. In the United States, the fasting glucose level for hypoglycemia is below 70 mg/dl ; the range of $70 - 99 \text{ mg/dl}$ is considered as euglycemia (normal concentration of glucose in the blood); and a fasting blood glucose level exceeding 126 mg/dl is diagnosed as diabetes, while the level of $100 - 125 \text{ mg/dl}$ is considered as prediabetes. The normal range for fasting insulin level may slightly vary across laboratories. In this study, we consider the reference range for normal fasting insulin level to be $5 - 25 \mu\text{U/mL}$, with $I \geq 25 \mu\text{U/mL}$ serving as the indication for hyperinsulinemia [2]. Throughout the numerical investigations, we interpret the simulation results based on the aforementioned definitions.

Figure 1 displays the normal levels of glucose and insulin, utilizing the parameter values outlined in Table 1 (in which $a = 6.27$ and $c = 0.0005$) and an initial condition of $(G, I) = (100 \text{ mg/dl}, 10 \mu\text{U/mL})$ during a fasting state. By modifying the value of the maximum production rate of insulin a while keeping the other parameters constant, we explore the impact of insulin secretion function on glucose metabolism.

The simulation results of model (2.3) with impaired insulin secretion ($a = 0.27$), as depicted in Figure 2 panels (a)–(b), illustrate that a reduced insulin secretion rate leads to insulin deficiency, resulting in a continual elevation of the individual’s glucose levels indicative of developing diabetes. Conversely, the simulation results of model

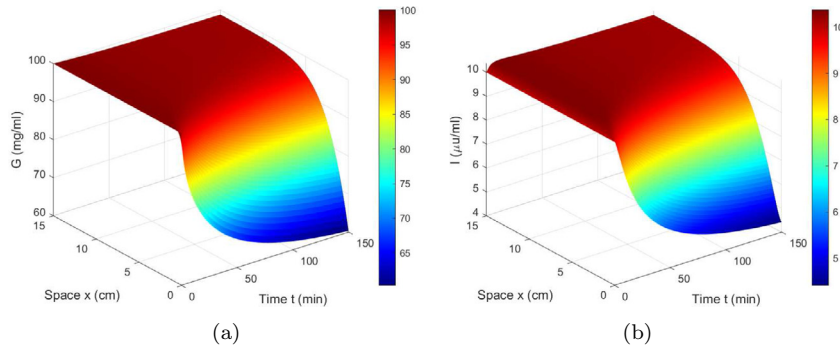


FIG. 1. Dynamics of glucose $G(x,t)$ and insulin $I(x,t)$ with the parameter set in Table 1 and the initial condition of $(G, I) = (100 \text{ mg/dl}, 10 \text{ } \mu\text{U/mL})$.

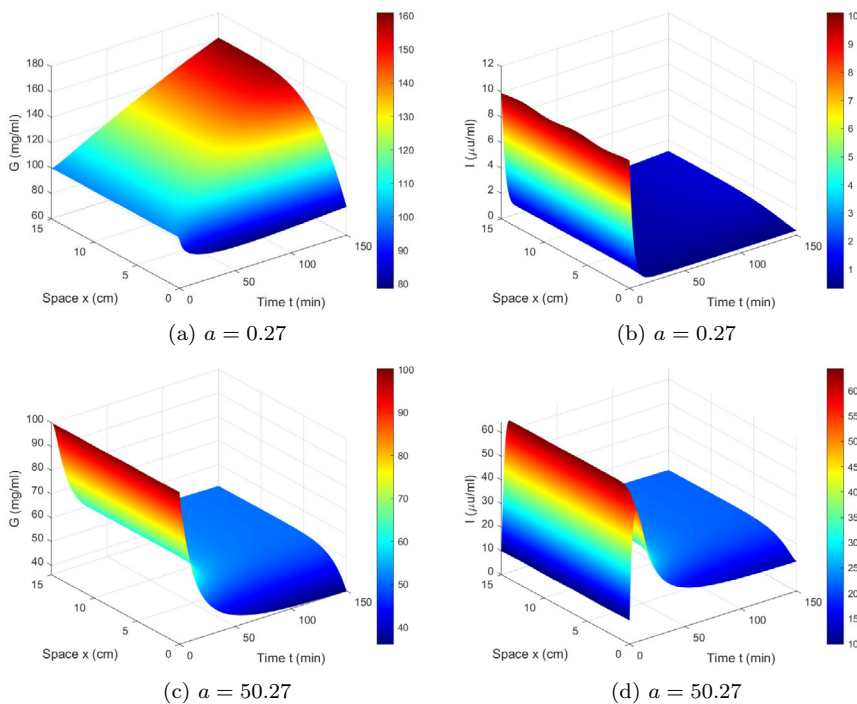


FIG. 2. Dynamics of glucose and insulin with different insulin secretion functions. (a)–(b) Impaired insulin secretion when $a = 0.27$. (c)–(d) Excessive insulin secretion when $a = 50.27$. The other parameters are in Table 1 and the initial condition of $(G, I) = (100 \text{ mg/dl}, 10 \text{ } \mu\text{U/mL})$.

(2.3) with excessive insulin secretion ($a = 50.27$), shown in Figure 2 panels (c)–(d), demonstrate that a rapid and substantial increase in insulin secretion rate causes a sharp rise in insulin levels, progressing to the hyperinsulinemic stage. Consequently, the glucose level progressively decreases, leading to severe hypoglycemic reactions with levels reaching approximately 60 mg/dl . The steady state concentration of glucose and insulin with different insulin secretion rates are shown in Figure 3.

By varying the value of insulin sensitivity c while keeping the other parameters constant, we investigate the impact of insulin sensitivity on glucose metabolism. Reduced insulin sensitivity, also known as insulin resistance, refers to a state in which

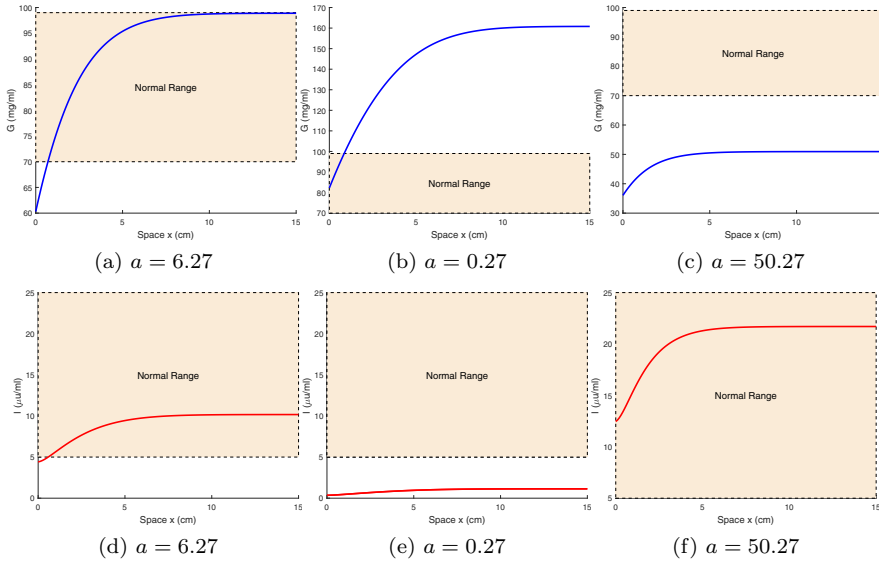


FIG. 3. Steady states of glucose and insulin with different insulin secretion functions. (a)–(c) Steady states of glucose when $a = 6.27, a = 0.27,$ and $a = 50.27$. (d)–(f) Steady states of insulin when $a = 6.27, a = 0.27,$ and $a = 50.27$. The other parameters are in Table 1 and the initial condition of $(G, I) = (100 \text{ mg/dl}, 10 \text{ } \mu\text{U/mL})$.

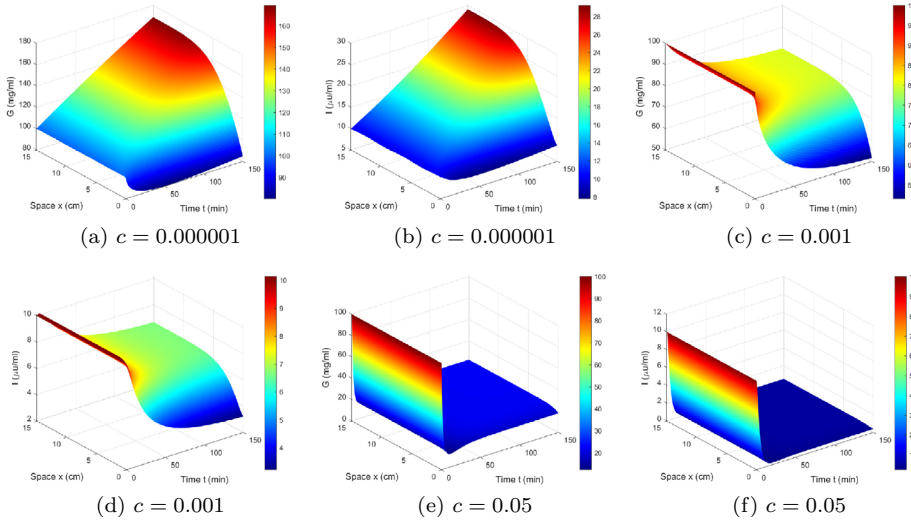


FIG. 4. Dynamics of glucose and insulin with different sensitivity. (a)–(b) Insulin resistance when $c = 0.000001$. (c)–(d) Slightly high insulin sensitivity when $c = 0.001$. (e)–(f) Excessive insulin sensitivity when $c = 0.05$. The other parameters are in Table 1 and the initial condition of $(G, I) = (100 \text{ mg/dl}, 10 \text{ } \mu\text{U/mL})$.

the target organ of insulin action becomes less responsive to its effects. This means that a normal dose of insulin produces a biological effect that is lower than normal. In Figure 4 panels (a)–(b), we present the simulation results of model (2.3) with insulin resistance ($c = 0.000001$). These results demonstrate that even in the absence of insulin deficiency (with insulin levels ranging from $10 - 29.3 \text{ } \mu\text{U/mL}$), glucose levels remain elevated, reaching up to 175 mg/dl . This indicates the persistence of elevated

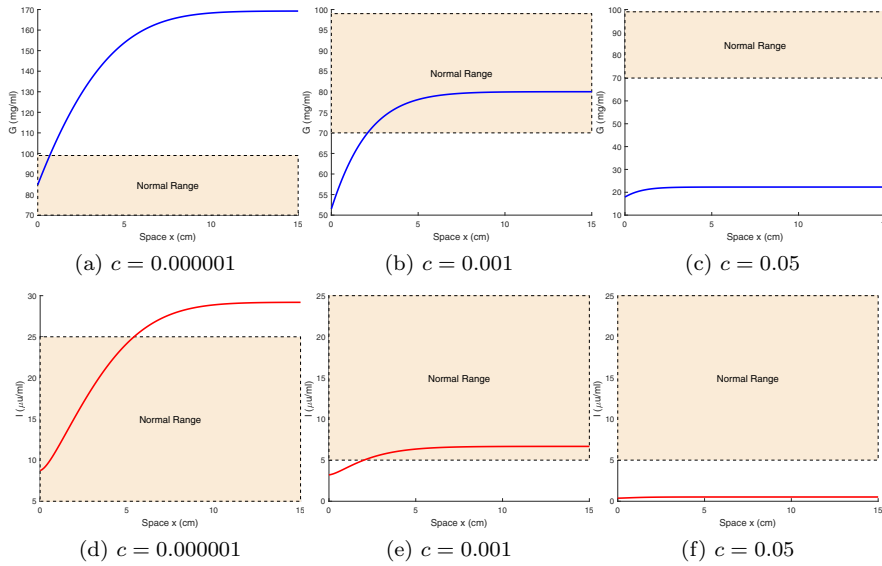


FIG. 5. Steady states of glucose and insulin with different sensitivity. (a)–(c) Steady states of glucose when $c = 0.000001$, $c = 0.001$, and $c = 0.05$. (d)–(f) Steady states of insulin when $c = 0.000001$, $c = 0.001$, and $c = 0.05$. The other parameters are in Table 1 and the initial condition of $(G, I) = (100 \text{ mg/dl}, 10 \text{ } \mu\text{U/mL})$.

blood glucose levels despite sufficient insulin production. Slightly increased insulin sensitivity ($c = 0.001$) has minimal impact on blood glucose and insulin concentrations, as depicted in Figure 4 panels (c)–(d). However, excessive insulin sensitivity ($c = 0.05$) can potentially lead to hypoglycemia, as shown in Figure 4 panels (e)–(f). The steady states of glucose and insulin with different insulin sensitivity are shown in Figure 5.

4.2. Spatio-temporal sensitivity and correlation. The intricacy and diversity of glucose metabolism pose significant challenges in understanding the corresponding responses of physiological parameters. To address this complexity and identify the key factors that influence glucose metabolism, we use the following two quantitative values: the spatio-temporal sensitivity index and correlation index. These analytical tools play a crucial role in unraveling the intricate relationships between parameters and provide valuable insights into their impact on glucose metabolism. By utilizing these quantities, we can gain a better understanding of the dynamic nature of glucose metabolism and explore the interplay among various factors involved in its regulation.

Sensitivity analysis (SA) serves as a means to reduce the complexity of the system and uncover high-impact parameters that warrant further investigation in subsequent studies [25]. In this study, we conduct SA using the normal parameter set outlined in Table 1. Relative sensitivity indices are employed, which involve evaluating the sensitivity of the model output to variations in parameters at different values, typically 10% of the baseline values. These indices are computed by multiplying the partial derivative (the absolute sensitivity function) by the input and dividing it by the output value. Consequently, the spatial sensitivity index (SI) $SI(x, t, \eta)$ of the model output to parameter variations can be determined for the normal parameter set:

$$SI(x, t, \eta) = \frac{\eta + \Delta\eta}{U(x, t, \eta + \Delta\eta)} \frac{[U(x, t, \eta + \Delta\eta) - U(x, t, \eta)]}{\Delta\eta},$$

where $U = G, I$, and the parameter η is one of $d_G, d_I, v_G, v_I, G_{in}, a, \mu_G, \mu_I, c, m$. The spatial sensitivity index $SI(x, t, \eta)$ allows us to assess the influence of parameter variations on the model's output, providing valuable insights into the dynamics of glucose metabolism.

In Figure 6, we depict the spatiotemporal variation of the SI in response to changes in physiological parameters. The absolute sensitivity indices of glucose (G) and insulin (I) with respect to μ_I, c, G_{in} , and a are significantly higher compared to other parameters. This observation suggests that these parameters play a dominant role in the interactions governing glucose homeostasis. Conversely, the low sensitivity of parameters v_I and d_I indicates that variations in these values would have minimal impact on glucose-insulin dynamics.

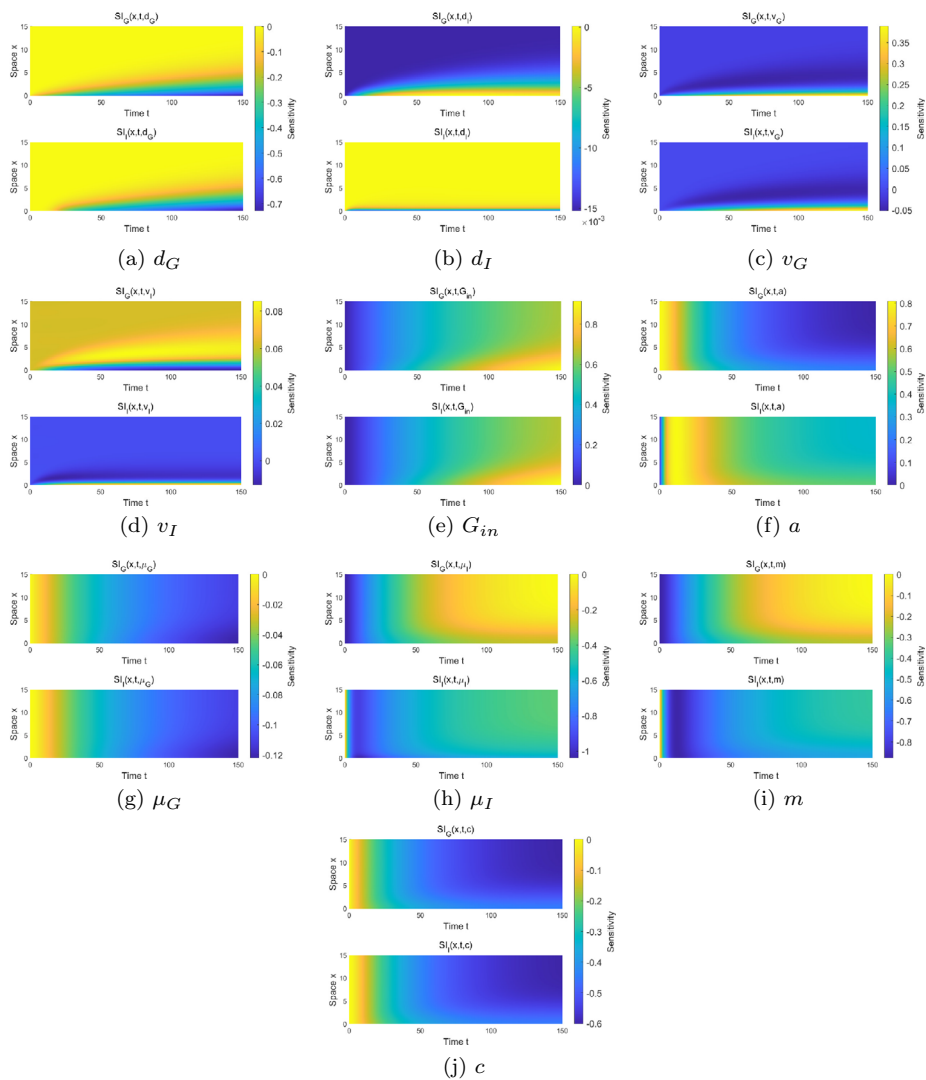


FIG. 6. Spatio-temporal sensitivity of $G(x, t)$ and $I(x, t)$ for the normal set parameters in Table 1 and the initial condition of $(G, I) = (100 \text{ mg/dl}, 10 \text{ } \mu\text{U/mL})$.

Downloaded 04/10/25 to 128.239.108.97 . Redistribution subject to SIAM license or copyright; see https://epubs.siam.org/terms-privacy

The investigation of parameter correlations involves computing the correlation between dynamic sensitivities, as outlined in previous studies [24, 25]. These correlations play a significant role in understanding the relationships between parameters and can guide the development of advanced treatment approaches. For example, when certain parameters are hard to regulate during therapeutic interventions, one can regulate the parameters highly correlated to them to indirectly achieve the regulation goal. By analyzing the correlated or anticorrelated parameters, doctors can explore alternative strategies for adjusting these parameters. The correlation matrix is commonly defined by the following term:

$$(4.1) \quad r_{ij} = \frac{\sum_{p=1}^M \sum_{q=1}^N (SI_{pq}^i - \overline{SI}_{pq}^i)(SI_{pq}^j - \overline{SI}_{pq}^j)}{\sqrt{\left(\sum_{p=1}^M \sum_{q=1}^N (SI_{pq}^i - \overline{SI}_{pq}^i)^2\right) \left(\sum_{p=1}^M \sum_{q=1}^N (SI_{pq}^j - \overline{SI}_{pq}^j)^2\right)}},$$

where $\overline{SI}_{pq}^{i,j}$ are the mean of $SI_{pq}^{i,j}$, p is space grid, q is time step grid, with $1 \leq p \leq M$, $1 \leq q \leq N$, $1 \leq i, j \leq 10$ (we consider the effect of 10 parameters here). The correlations are shown in Figures 7 and 8 from positive correlated (+1) to anti-correlated (-1).

In Figure 7 panel (a), we observe the correlations between the dynamic sensitivities of glucose for the parameters listed in Table 1. A strong positive correlation is found between the sensitivities of parameters c and μ_G . This indicates a “compensatory effect of feedback to insulin resistance,” where a high value of μ_G is required to maintain glucose levels within the normal range when c is low. A similar compensatory feedback is also observed between m and μ_I . When m is low, a high value of μ_I is needed to ensure that insulin fluctuates within the normal range, thus maintaining blood sugar levels within the normal range. A significantly high negative correlation is observed between the pairs of parameters c, G_{in} , and μ_G, G_{in} , suggesting that a high insulin sensitivity or a noninsulin-mediated glucose uptake rate is necessary to maintain normal glucose levels when the net hepatic glucose production rate is high. Similar anticorrelations are observed between the pairs of parameters μ_I, m and μ_I, a . In Figure 7 panel (b), we find the correlations between the dynamic sensitivities

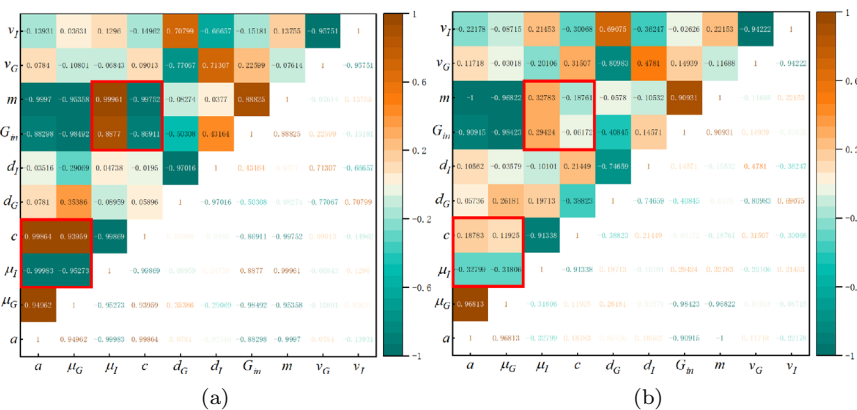


FIG. 7. (a) Correlations between dynamic sensitivities of glucose for parameters in Table 1. (b) Correlations between dynamic sensitivities of glucose when $a = 0.07$ and other parameters in Table 1. (Figure in color online.)

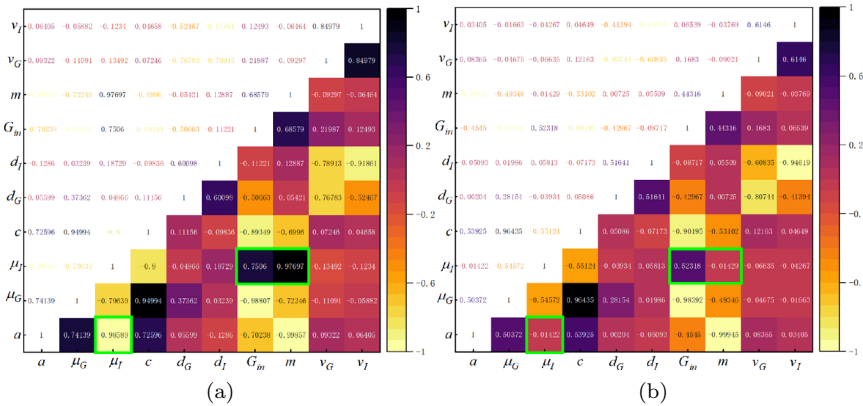


FIG. 8. (a) Correlations between dynamic sensitivities of glucose for parameters in Table 1. (b) Correlations between dynamic sensitivities of glucose when $\mu_I = 4.5$ and other parameters in Table 1.

of glucose for $a = 0.07$ and other parameters listed in Table 1. When normal physiological parameters change, the initially highly correlated feedback regulatory processes (in the red box of Figure 7) are influenced, resulting in a significant decrease in the absolute value of the correlation.

Figure 8 panel (a) displays the correlations between the dynamic sensitivities of insulin for the parameters listed in Table 1. Similar to glucose, a “compensatory effect of feedback to insulin resistance” is observed through a strong positive correlation between parameters c and μ_G . This suggests that a compensatory feedback mechanism operates to maintain normal insulin levels when insulin resistance is present. Such feedback is also found between parameters m and μ_I . Additionally, a highly negative correlation is observed between parameters a and μ_I , indicating that a high insulin production rate is necessary to maintain normal insulin levels when the clearance rate is high. In Figure 8 panel (b), we have the correlations between the dynamic sensitivities of glucose for $\mu_I = 4.5$ and other parameters listed in Table 1. When μ_I is increased, the previously highly correlated feedback between the pairs of parameters $a, \mu_I, \mu_I, m,$ and μ_I, G_{in} is affected, resulting in changes in the correlations between these parameters.

5. Conclusion. In this paper, we propose a reaction-diffusion-advection model for glucose metabolism in the pancreatic islet, aiming to capture its spatiotemporal behaviors. We investigate the global existence and boundedness of the model’s solution, as well as establish the uniqueness of its positive steady state. Moreover, we introduce formulas for spatiotemporal sensitivity index and correlation index to identify significant physiological factors and illustrate parameter interdependency. Additionally, we conduct simulations to analyze the dynamics of the system across various stages, including hyperinsulinemia, hypoglycemia, euglycemia, and diabetes. These findings offer valuable insights and guidance for therapeutic interventions, facilitating the development of effective treatments.

This work represents the first step of establishing a spatial dynamic model for glucose-insulin metabolism. Various previous works [14, 23, 21, 2] have considered the time-delays within the glucose regulation process, and our current study has not incorporated time-delays which is a limitation of our model. A potential future

direction would be to include spatiotemporal delays (weighted spatial-average delay terms) into the diffusive glucose-insulin model, while considering both diffusion and delay effects.

REFERENCES

- [1] S. CARVALHO, N. GUEIRAL, E. NOGUEIRA, R. HENRIQUE, L. OLIVEIRA, AND V. TUCHIN, *Glucose diffusion in colorectal mucosa—a comparative study between normal and cancer tissues*, J. Biomed. Opt., 22 (2017), 091506, <https://doi.org/10.1117/1.JBO.22.9.091506>.
- [2] R. B. COHEN AND J. X. LI, *A novel model and its analysis on the metabolic regulations of glucose, insulin, and glucagon*, SIAM J. Appl. Math., 81 (2021), pp. 2684–2703, <https://doi.org/10.1137/21M1390876>.
- [3] A. DE GAETANO, T. HARDY, B. BECK, E. ABU-RADDAD, P. PALUMBO, J. BUE-VALLESKEY, AND N. PØRKSEN, *Mathematical models of diabetes progression*, Am. J. Physiol. Endocrinol. Metab., 295 (2008), pp. E1462–E1479, <https://doi.org/10.1152/ajpendo.90444.2008>.
- [4] M. M. ENGELGAU, K. M. NARAYAN, AND W. H. HERMAN, *Screening for type 2 diabetes*, Diabetes Care, 23 (2000), pp. 1563–1580, <https://doi.org/10.2337/diacare.23.10.1563>.
- [5] F. FATEHI, A. MENON, AND D. BIRD, *Diabetes care in the digital era: A synoptic overview*, Curr. Diab. Rep., 18 (2018), 38, <https://doi.org/10.1007/s11892-018-1013-5>.
- [6] L. A. FERRAT, K. VEHIK, S. A. SHARP, Å. LERNMARK, M. J. REWERS, J. X. SHE, A. G. ZIEGLER, J. TOPPARI, B. AKOLKAR, J. P. KRISCHER, M. N. WEEDON, R. A. ORAM, W. A. HAGOPIAN, AND TEDDY Study Group, *A combined risk score enhances prediction of type 1 diabetes among susceptible children*, Nat. Med., 26 (2020), pp. 1247–1255, <https://doi.org/10.1038/s41591-020-0930-4>.
- [7] N. R. GANDASI AND S. BARG, *Contact-induced clustering of syntaxin and munc18 docks secretory granules at the exocytosis site*, Nat. Commun., 5 (2014), 3914, <https://doi.org/10.1038/ncomms4914>.
- [8] J. HA, L. S. SATIN, AND A. S. SHERMAN, *A mathematical model of the pathogenesis, prevention, and reversal of type 2 diabetes*, Endocrinology, 157 (2015), pp. 624–635, <https://doi.org/10.1210/en.2015-1564>.
- [9] B. M. HENRY, B. SKINNINGSRUD, K. SAGANIAK, P. A. PÉKALA, J. A. WALOCHA, AND K. A. TOMASZEWSKI, *Development of the human pancreas and its vasculature—An integrated review covering anatomical, embryological, histological, and molecular aspects*, Ann. Anat., 221 (2019), pp. 115–124, <https://doi.org/10.1016/j.aanat.2018.09.008>.
- [10] C. HU, J. YANG, J. D. JOHNSON, AND J. LI, *Modeling the Distribution of Insulin in Pancreas*, preprint, <https://arxiv.org/abs/2406.00458>, 2024.
- [11] J. KANG, G. ERDODI, J. P. KENNEDY, H. CHOU, L. LU, AND S. GRUNDFEST-BRONIATOWSKI, *Toward a bioartificial pancreas: Diffusion of insulin and IgG across immunoprotective membranes with controlled hydrophilic channel diameters*, Macromol. Biosci., 10 (2010), pp. 369–377, <https://doi.org/10.1002/mabi.200900386>.
- [12] J. LÓPEZ-GÓMEZ AND R. PARDO, *Existence and uniqueness of coexistence states for the predator-prey model with diffusion: The scalar case*, Differential Integral Equations, 6 (1993), pp. 1025–1031, <https://doi.org/10.57262/die/1370021908>.
- [13] R. MUNIYAPPA AND K. J. WILKINS, *Diabetes, obesity, and risk prediction of severe COVID-19*, J. Clin. Endocrinol. Metab., 105 (2020), pp. e3812–e3814, <https://doi.org/10.1210/clinem/dgaa442>.
- [14] A. L. MURILLO, J. X. LI, AND C. CASTILLO-CHAVEZ, *Modeling the dynamics of glucose, insulin, and free fatty acids with time delay: The impact of bariatric surgery on type 2 diabetes mellitus*, Math. Biosci. Eng., 16 (2019), pp. 5765–5787, <https://doi.org/10.3934/mbe.2019288>.
- [15] T. C. NICHOLS, E. P. MERRICKS, D. A. BELLINGER, R. A. RAYMER, J. YU, D. LAM, G. G. KOCH, W. H. BUSBY, AND D. R. CLEMMONS, *Oxidized LDL and fructosamine associated with severity of coronary artery atherosclerosis in insulin resistant pigs fed a high fat/high NaCl diet*, PloS One, 10 (2015), e0132302, <https://doi.org/10.1371/journal.pone.0132302>.
- [16] L. R. NYMAN, E. FORD, A. C. POWERS, AND D. W. PISTON, *Glucose-dependent blood flow dynamics in murine pancreatic islets in vivo*, Am. J. Physiol. Endocrinol. Metab., 298 (2010), pp. E807–E814, <https://doi.org/10.1152/ajpendo.00715.2009>.
- [17] K. OGURTSOVA, J. D. DA ROCHA FERNANDES, Y. HUANG, U. LINNENKAMP, L. GUARIGUATA, N. H. CHO, D. CAVAN, J. E. SHAW, AND L. E. MAKAROFF, *IDF diabetes atlas: Global estimates for the prevalence of diabetes for 2015 and, 2040*, Diabetes Res. Clin. Pract., 128 (2017), pp. 40–50, <https://doi.org/10.1016/j.diabres.2017.03.024>.

- [18] M. OHARA-IMAIZUMI, T. FUJIWARA, Y. NAKAMICHI, T. OKAMURA, Y. AKIMOTO, J. KAWAI, S. MATSUSHIMA, H. KAWAKAMI, T. WATANABE, K. AKAGAWA, AND S. NAGAMATSU, *Imaging analysis reveals mechanistic differences between first-and second-phase insulin exocytosis*, *J. Cell Biol.*, 177 (2007), pp. 695–705, <https://doi.org/10.1083/jcb.200608132>.
- [19] M. OHARA-IMAIZUMI AND S. NAGAMATSU, *Insulin exocytotic mechanism by imaging technique*, *J. Biochem.*, 140 (2006), pp. 1–5, <https://doi.org/10.1093/jb/mvj127>.
- [20] C. V. PAO, *Nonlinear Parabolic and Elliptic Equations*, Plenum Press, New York, 1992.
- [21] F. RAO, Z. L. ZHANG, AND J. X. LI, *Dynamical analysis of a glucose-insulin regulatory system with insulin-degrading enzyme and multiple delays*, *J. Math. Biol.*, 87 (2023), 73, <https://doi.org/10.1007/s00285-023-02003-6>.
- [22] P. V. RÖDER, B. B. WU, Y. X. LIU, AND W. P. HAN, *Pancreatic regulation of glucose homeostasis*, *Exp. Mol. Med.*, 48 (2016), e219, <https://doi.org/10.1038/emm.2016.6>.
- [23] X. Y. SONG, M. Z. HUANG, AND J. X. LI, *Modeling impulsive insulin delivery in insulin pump with time delays*, *SIAM J. Appl. Math.*, 74 (2014), pp. 1763–1785, <https://doi.org/10.1137/130933137>.
- [24] K. SRIRAM, M. RODRIGUEZ-FERNANDEZ, AND F. J. DOYLE, III, *Modeling cortisol dynamics in the neuro-endocrine axis distinguishes normal, depression, and post-traumatic stress disorder (PTSD) in humans*, *PLoS Comput. Biol.*, 8 (2012), e1002379, <https://doi.org/10.1371/journal.pcbi.1002379>.
- [25] Y. W. TAO, Y. T. SUN, H. P. ZHU, J. N. LYU, AND J. L. REN, *Nilpotent singularities and periodic perturbation of a $G\beta$ model: A pathway to glucose disorder*, *J. Nonlinear Sci.*, 33 (2023), 49, <https://doi.org/10.1007/s00332-023-09907-z>.
- [26] C. TARIN, E. TEUFEL, J. PICÓ, J. BONDIA, AND H. J. PFLEIDERER, *Comprehensive pharmacokinetic model of insulin glargine and other insulin formulations*, *IEEE. Trans. Biomed. Eng.*, 52 (2005), pp. 1994–2005, <https://doi.org/10.1109/TBME.2005.857681>.
- [27] B. TOPP, K. PROMISLOW, G. DEVRIES, R. M. MIURA, AND D. FINEGOOD, *A model of β -cell mass, insulin, and glucose kinetics: Pathways to diabetes*, *J. Theoret. Biol.*, 206 (2000), pp. 605–619, <https://doi.org/10.1006/jtbi.2000.2150>.
- [28] G. C. WAKE, A. B. PLEASANTS, M. H. VICKERS, A. M. SHEPPARD, AND P. D. GLUCKMAN, *The application of a model of glucose and insulin dynamics to explain an observed effect of leptin administration in reversal of developmental programming*, *Math. Biosci.*, 229 (2011), pp. 109–114, <https://doi.org/10.1016/j.mbs.2010.11.005>.
- [29] Y. WANG, J. P. SHI, AND J. F. WANG, *Persistence and extinction of population in reaction-diffusion-advection model with strong Allee effect growth*, *J. Math. Biol.*, 78 (2019), pp. 2093–2140, <https://doi.org/10.1007/s00285-019-01334-7>.
- [30] Y. F. WANG, S. ČANIĆ, M. BUKAČ, C. BLAHA, AND S. ROY, *Mathematical and computational modeling of poroelastic cell scaffolds used in the design of an implantable bioartificial pancreas*, *Fluids*, 7 (2022), 222, <https://doi.org/10.3390/fluids7070222>.
- [31] J. XIE, M. WANG, Z. LONG, H. NING, J. LI, Y. CAO, Y. LIAO, G. LIU, F. WANG, AND A. PAN, *Global burden of type 2 diabetes in adolescents and young adults, 1990-2019: Systematic analysis of the global burden of disease study 2019*, *Bmj*, 379 (2022), e072385, <https://doi.org/10.1136/bmj-2022-072385>.
- [32] D. ZHU, E. KOO, E. KWAN, Y. KANG, S. PARK, H. XIE, S. SUGITA, AND H. Y. GAISANO, *Syntaxin-3 regulates newcomer insulin granule exocytosis and compound fusion in pancreatic beta cells*, *Diabetologia*, 56 (2013), pp. 359–369, <https://doi.org/10.1007/s00125-012-2757-0>.